1/17/80

DR. 1036

LA-7684-MS

Informal Report

MASTER

An Opacity Test Using a Neon-Seeded Theta Pinch

University of California

LOS ALAMOS SCIENTIFIC LABORATORY

Post Office Box 1663 Los Alamos, New Mexico 87545

LA-7684-MS
Informal Report
UC-20
Issued: February 1980

An Opacity Test Using a Neon-Seeded Theta Pinch

D. B. Thomson

CONTENTS

AN OPACITY TEST USING A NEON-SEEDED THETA PINCH

by

D. B. THOMSON

ABSTRACT

Vacuum ultraviolet (VUV) emission from a neon-seeded high-density θ-pinch has been observed for comparison with theoretical radiation emission calculations. The plasma was created in a 25-cm-long θ-coil with 90-kG field having a 3.0-μs quarter period. A gas fill of 1 torr of helium + 2% neon was used. Observation of the HeII 4686 line/continuum ratio gave an electron temperature of 25 ± 4 eV. Shadowgraphs of the plasma radius, taken with a ruby laser, gave an electron density of $0.9 \pm 0.09 \times 10^{18}$ cm^{-3}. The VUV emission was observed in radial view and with time resolution with a 2.2-m grazing-incidence monochromator equipped with a photomultiplier and p-terphenyl scintillator. Thin foils of carbon and aluminum were used as filters to absorb stray light and pass emission in the 44- to 100-A region.

Relative emission intensities from the Ne VIII transitions 2p - 7d,s, 2p - 6d,s, 2p - 5d,s, 2s - 5p, 2s - 4p, and 2p - 4d were obtained. Analysis of these levels gave a temperature of 27 eV and indicated an approach to LTE.

A detailed search was made of the 50- to 60-A region for the Ne VIII 2p free-bound recombination edge. It was not observed and analysis indicates that the free-bound cross section must be approximately equal to or less than that given by the opacity code used.

I. INTRODUCTION

The calculation of opacities of matter at plasma temperatures has long been important in astrophysics and is very essential to other high-temperature plasma applications such as laser fusion. Most tests of the opacity calculations are complicated by the need to use hydrodynamics to

analyze the data. Thus, in the 30 years that such opacities have been calculated,[1,2,3] there have been virtually no experiments that directly test the opacity models themselves, for high-temperature plasmas (T_e > 10 eV) involving multiple stages of ionization.

In earlier feasibility[4] experiments with the Scyllar θ-pinch using gas fills of helium plus several per cent neon at about 1 torr we observed a plasma for which $T_e \sim 40$ eV, $n_e \sim 5 \times 10^{17}$ electrons cm^{-3}, and for which Ne VIII appeared to be a major constituent. It was suggested by A. L. Merts[5] that observation of the strength of the 2p free-bound recombination edge of Ne VIII in a plasma such as this could demonstrate a test of the models used for opacity calculations, if the electron temperature and density were measured accurately and the appropriate equilibrium conditions were satisfied.

In earlier experiments,[4,6] the vacuum ultraviolet (VUV) emission from the high stages of ionization was recorded on film. The present experiment[7] represents the only attempt to apply time-resolved VUV spectroscopy to the Scyllar θ-pinch when it was operated at sufficient density and temperature to do the suggested neon opacity experiment.[5,8]

II. THEORY

A. The Absorption Cross Section and Opacities

Theoretical models used for opacity calculations include the calculation of the cross section for the absorption of a photon by an atomic system

$$\sigma_{ij} \propto \langle \psi_i | r | \psi_j \rangle^2 \quad , \tag{1}$$

where ψ_i and ψ_j are the wave functions for the lower and upper atomic states, respectively.

Processes contributing[3] to the absorption are primarily bound-bound, bound-free, and inverse bremsstrahlung. In the first case, an electron in a bound state of the atom is excited to another bound state by absorption of the incident photon. This is the familiar line absorption. In the second case, the bound state electron is removed from the atom, going into one of the continuum of free states available, that is, photoionization. In contrast to line absorption, this process is possible for any energy of

the incident quantum greater than the ionization energy of the atom. Lastly, an electron in a free state may absorb a photon by a transition to another free state in the presence of a third body such as an ion. Any amount of energy may be absorbed by this process. The inverse processes to these three absorption processes are the following: line emission, radiative recombination, and bremsstrahlung. Each of these processes may be important for atoms immersed in high-temperature high-density plasmas and each is dependent on the temperature, density, and atomic species. In such plasmas the high-Z elements will be partially or highly stripped and in general all three processes contribute to the opacity.

In many cases the bound-free process is a major contributor to the opacity, particularly when many photoionization edges are present and overlap, or cover an important region of the spectrum for some particular temperature or range of temperatures. In these cases, the ψ_j for the upper states of Eq. (1) are particularly important to the opacity calculations and are model dependent. Thus the cross sections need[5,8] to be tested by experiment for highly ionized atoms in high-temperature plasmas. In the present work a selected bound-free edge was sufficiently removed from neighboring lines and edges so that it could be studied in an unambiguous manner, independent of other processes. The 2p and 2s edges of Ne VIII occur at about 55.7 and 51.8 A, respectively. In the feasibility experiments,[4] this region of the observed spectra was well isolated from lines of other stages of ionization and impurities.

B. Emission Spectra and the Recombination Edge in Ne VIII

The absorption cross section σ_{ij} can be related to the observed emission spectra by using formulas given by Griem.[9] Assuming LTE, the emission intensity may be expressed as

$$I(\omega) \propto \omega^3 \exp\left(\frac{-h\omega}{KT_e}\right)\left[\frac{1}{(KT_e)^{3/2}}\right]\exp\left(\frac{E_{ion}}{KT_e}\right)\exp\left(\frac{-E_i}{KT_e}\right)(n_e N_j' \sigma_{ij} g_i/g_j') \quad ,(2)$$

where $I(\omega)$ is the radiated power per unit solid angle per unit frequency interval and T_e = electron temperature, E_{ion} = ionization energy, n_e = electron density, E_i = energy of lower level above-ground state, (ω) = emission frequency, σ_{ij} = absorption cross section, i,j = lower and

upper states, $N_{j'}$ = number density of ions in the ground state of the higher ionic state (Ne IX), and g_i and $g_{j'}$ are the statistical weights.

Opacity codes[1,2] may be used to calculate σ_{ij} for bound-bound, bound-free, and free-free transitions. We can use Eq. (2) to determine the relative magnitudes, in emission, of observed b-b transitions to the expected magnitude of the b-f transitions from the calculated σ_{ij}.

Theoretical calculations for the strengths of the absorption cross section σ_{ij} were made by Merts and Magee[8] for the case of a helium + 2% neon plasma at the electron temperature of 25 eV and density of $\sim 10^{18}$ cm^{-3}. They used polynomial solutions of the Schrodinger equation and applied them to the calculation of cross sections as described by Merts and Matudka.[10]

Using these [illegible] for σ_{ij} and using Eq. (2), we calculated the expected re[illegible] intensities of the Ne VIII 2p and 2s bound-free edges rela[illegible]ities of the 2p - 5d,s, the 2p - 6d,s, and other nea[illegible].

Figu[illegible]t of the calculation. The theoretical relative i[illegible].he Ne VIII 2p lines with upper states from n = 5 to n = [illegible].es from n = 4 to n = 7; and the 2p and 2s free bound edges are s[illegible]n Fig. 1.

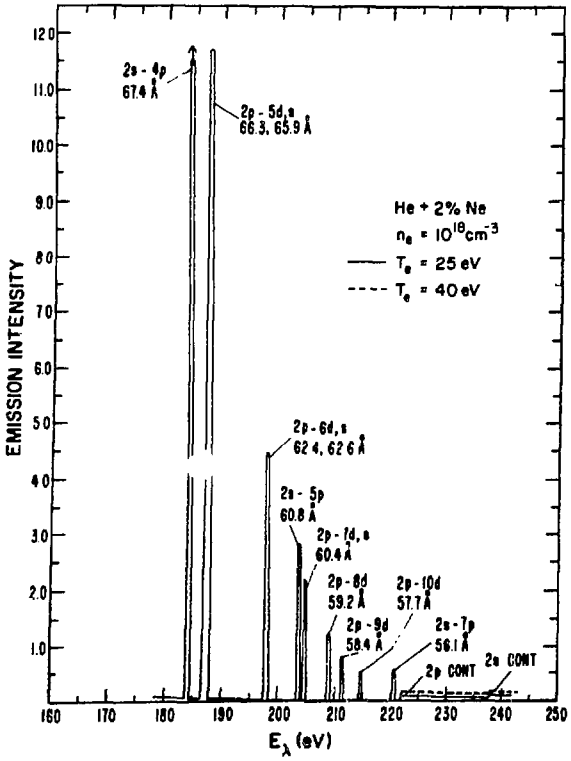

Fig. 1. Theoretical emission vs photon energy for a neon-seeded plasma. The relative emission intensities are computed from Eq. (2) using absorption cross sections from the opacity code of Merts and Magee (Ref. 8). A plasma of helium + 2% neon was assumed with $n_e = 10^{18}$ cm^{-3}. The solid line is for T_e = 25 eV, and the dashed line is for T_e = 40 eV.

C. The LTE Requirement

Use of Eq. (2) for a particular species requires[9] that the population of the upper level for each line transition be in LTE with respect to all higher levels of the same ionization stage and the ground state of the next higher ionization stage. LTE requires detailed balance between the levels in question.

In an optically thin plasma, in which we can ignore the reabsorption of radiation, LTE occurs only if the collisional rate processes dominate the radiative processes.

This condition is especially stringent for low-lying levels because their radiative lifetimes are short and their collisional cross sections are small. For almost all levels, cross sections for excitation are much larger than those for de-excitation. Therefore, near or in LTE, the population of a given level is determined mostly by the balance between collision induced de-excitation from higher levels and collisional excitation from this level into the higher levels.

The population of the level is thus in LTE with respect to all higher levels if its total transition probability for radiative decay is considerably smaller than the total rate of collisional excitation from this level to all higher levels. In equilibrium this is the same as the rate of its collisional population from the higher levels.

By calculating an average radiative decay rate of states with principal quantum number n and comparing it with the collisional transition rate per ion in state n to state n' $\langle \sigma_{n'n} v \rangle_{ave} n_e$, Greim[9] obtains a condition for LTE,

$$n_e \geq 7 \times 10^{18} \frac{Z^7}{n^{17/2}} \left(\frac{KT_e}{Z^2 E_H} \right)^{1/2} \left(cm^{-3} \right) , \qquad (3)$$

where n_e = electron density, n = principal quantum number, Z = effective charge acting on the radiating electron, T_e = electron temperature, and E_H = ionization energy of hydrogen.

The satisfaction of Eq. (3) requires a collisional rate 10 times greater than the average radiative rate.

If we use $n_e \sim 10^{18}$ and $T_e \leq 40$ eV in Eq. (3), we find that the LTE requirement should be satisfied for all $n \geq 5$ for the case of neon (VIII) shown in Fig. 1.

III. OBSERVATIONS WITH A NEON-SEEDED THETA PINCH

A. The Scyllar Theta Pinch

A θ-pinch plasma source was used for these experiments. It was driven by an axial field of ∿90 kG, with a risetime (quarter period) of 3.0 μs in a 25-cm-long, 8.2-cm-i.d. θ-coil. The energy for the θ-pinch was a low-inductance high-energy (∿180 kJ) capacitor bank consisting of 54 capacitors (60 kV, 1.8 μF), each switched with a low-inductance 4-electrode spark gap. In the feasibility experiments,[4] the θ-pinch typically was operated with gas fills of 1-2 torr of deuterium or helium and seeded with a few percent neon or other high-Z element to be studied. The emission spectra,[11] mainly in the VUV, were observed on film as a function of the seed element and pinch conditions. This Scylla-like θ-pinch was called Scyllar to indicate the radiation studies for which it was dedicated.

In earlier experiments, a pulsed linear discharge of ∿ 20 kA was used for preionization and applied ∿37 μs before the start of the main axial drive field. Ceramic discharge tubes were used with the linear discharge preionization because of tube breakage when thin-walled (2-mm) quartz tubes were tried first.

In the present experiments, preionization was obtained with a $\dot{B}_z$ discharge from two capacitors (0.75 μf, 50 KV each) into the main θ-coil about 30 μs ahead of the main drive field. With this preionization and with a crowbar applied to the main bank current at the peak of the first quarter cycle, we could use thick-walled (4-mm) quartz tubes without breakage for hundreds of shots using the full bank. [The quartz tubes were used successfully for thousands of shots in other experiments where operation with only 1/3 the bank was required, and lower fill densities ($\leq$ 150 m torr) were used.]

Scyllar was used for a variety of experiments involving radiation studies and atomic processes in high-temperature plasmas. When it was operated with 18 capacitors (1/3 bank), several thousands of shots of plasma data were obtained per year with a minimum of bank maintenance. For this case, the axial drive field rose to 45 kG with a quarter period of 2.0 μs (crowbarred at peak current), in the standard θ-coil of length 25 cm and i.d. of 8.2 cm with the vacuum LOS radial viewing port.[4,11] In this mode of operation detailed data was obtained involving identification of lines and stages of ionization of the noble gases[12] and iron,[6] line broadening,[13]

collisional ionization rates,[14,15] and dielectronic recombination.[16] Figure 2 shows Scyllar as it was used for much of this earlier work.

B. Time-Resolved VUV Emission Near the Ne VIII 2p Recombination Edge

In the earlier experiments,[4] Scyllar was used at full bank with a gas fill of helium + 2% neon at ∿1 torr, to create a plasma of $n_e \sim 10^{18}$ cm^{-3} and $T_e \sim 40$ eV.

The θ-pinch was observed with a 2.2-m grazing-incidence vacuum spectrograph (Spex Industries, Inc.) using a vacuum LOS in radial view.

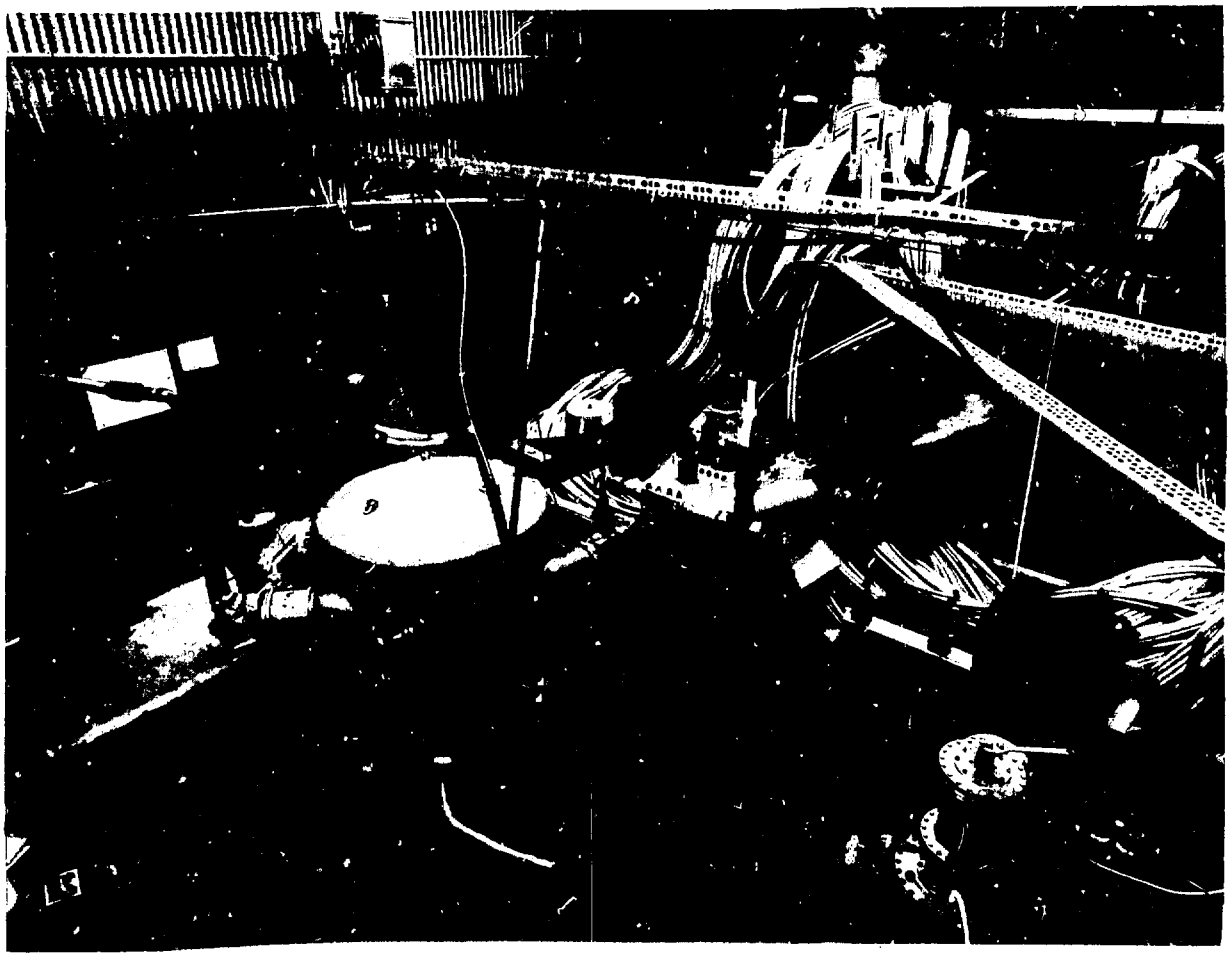

Fig. 2. The Scyllar θ-pinch with the 2.2-m grazing-incidence vacuum spectrometer (SPEX) positioned for radial view. The quartz tube that protudes from the θ-coil provides vacuum LOS to the spectrometer. The 60 kV - 180 kJ capacitor bank is in the upper right background.

The lines of Ne VIII from n = 3 to n = 6 were observed readily on film. The preponderant abundance of Ne VIII and Ne VII lines indicated a plasma sample homogeneous in temperature in radial view.[4,12] In subsequent work,[14] the VUV spectra was obtained with time resolution using a p-terphenyl scintillator and photomultiplier detector mounted to swing on the Rowland Circle in the spectrograph. The output of the photomultiplier was recorded on a 556 oscilloscope.

When using the photoelectric detector to look[17] for the weaker lines from higher lying levels, it was found necessary to use very thin foil filters of carbon, or carbon and aluminum, to attenuate the stray light level while passing the VUV lines in the region 45 to 90 A. Use of the thin film filters improved[17] the ratio of signal to stray light by a factor of 5 or better, at 65 A, for the case of Scyllar operated at 1/3 bank.

In the present work, a 2.2-m grazing-incidence vacuum monochromator (McPherson Model 247) was used to view the plasma radially, as shown in Fig. 3. A 1200 line/mm grating was used at an incident angle of 86°. The detector consisted of p-terphenyl scintillator sprayed on a glass plate attached to an RCA 8852 photomultiplier. The thin foil filters, carbon or carbon/aluminum, were supported on a transmission screen mounted* on aluminum holders and positioned just in front of the exit slit.

The thin film attenuations were computed using data given by Henke.[18] Figure 4 shows the transmission vs wavelength for the 60 mg cm^{-2} carbon foil used during the present work.

The primary search for the 2p bound-free edge was made with this arrangement. The θ-pinch was filled with helium + 2% neon at 1.0-torr pressure. The $\dot{B}_z$ preionization circuit (1.4 μf, 50 kV) was used, and full bank capacitance (97.2 μf) was used at 50 kV to give the 90-kG axial drive field (T/4 = 3.0 μs). The spectra were obtained by scanning, one shot at a time, given segments of the spectral region. Figure 5 shows typical time histories of two Ne VIII lines, the 88.11-A 2s-3p line and the 62.36-A 2p-6d line. It is seen that the Ne VIII emission was very sharply peaked, with the maximum occurring about 0.6 μs after start of the B field. The time histories of all the Ne VIII lines looked essentially the same.

Spectral scans were made over strong Ne VIII lines to check the calibration curve for the monochromator against dial settings at which these identified lines were observed. The calibration curve appeared to be

*Courtesy of Judith Gursky, P-7.

quite good ($\lesssim$0.5 A) over a wide range of the spectrum, 60 to 100 A, throughout the course of the work. Observation of the C V 40.27-A and the O VII 21.60-A lines in concurrent work[16] verified that the calibration curve was good down to those wavelengths. The wavelengths of resolved observed lines close to identified known lines could be determined to $\pm$0.2 A or better.

Figure 6 shows results of a detailed scan of the spectral region 66- to 50-A involving 43 shots of the θ-pinch. The θ-tube was pumped out and refilled with pure helium + 2% neon before each shot. For each data point, the amplitude of the photomultiplier signal was read at the peak of the signal, at t = 0.6 μs. In Fig. 6, signal amplitude is plotted against $E_\lambda = hc/\lambda = 12367/\lambda$ (A).

The monochromator slit width used for the spectral scan of Fig. 6 was chosen to be wide enough to get a substantial signal for each of the lines to be used for comparison purposes, yet narrow enough to provide adequate wavelength resolution to clearly resolve those lines. In Fig. 6 the resolution was 0.49 A. The background level observed between the lines was studied by taking several shots at wavelengths below the carbon edge ($\sim$43 A). If the background level was true emission continuum, it would be expected to increase by a factor of $\sim$5 at wavelengths just below the carbon edge, because of the thin film filter. The average increase for three such shots was about 10%, less than the normal shot-to-shot variations. It was concluded that most of the background signal was due to residual stray light from the plasma and grating.

Figure 7 shows a scan, similar to Fig. 6, but taken earlier with an older discharge tube, which had been used for many hundreds of shots in other experiments. The apparent stray light level in Fig. 7 is somewhat stronger than in Fig. 6 and may have been caused by light owing to a higher level of impurities from the walls of the older tube. No obvious jump in the continuum level, from the Ne VIII 2p recombination edge was observed in either Fig. 6, Fig. 7, or in the several preliminary partial scans that were taken.

In earlier work[4] at similar plasma conditions, the 2s-5p line (60.8 A) and the 2p-7d,s line (60.4 A) were resolved from each other on film, using a narrow slit on the vacuum spectrograph. In the scans of Figs. 6 and 7, their intensities are combined into one observed line by the 0.49-A resolution used for these scans.

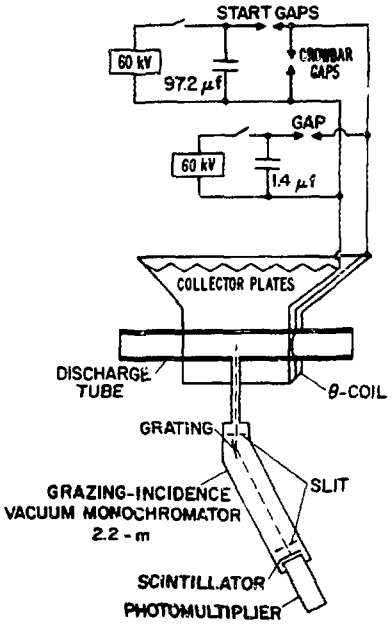

Fig. 3. The Scyllar θ-pinch with the McPherson Model 247 2.2-m grazing-incidence vacuum monochromater.

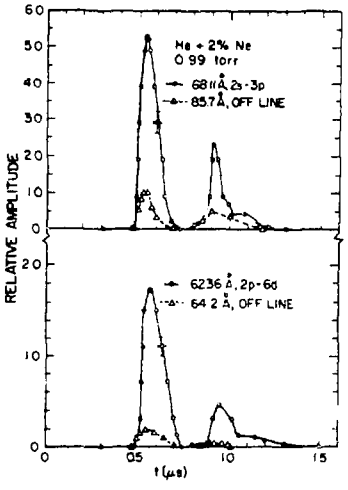

Fig. 5. Observed intensity vs time for Ne VIII lines obtained from oscilloscope traces of the photomultiplier output of the vacuum monochromater shown in Fig. 3. The θ-pinch source was operated at full bank capacitance, giving an axial drive field of 90-kG with a quarter period of 3.0 μs. The gas fill was helium + 2% neon at 1.0 torr. Time is measured from the start of the drive field.

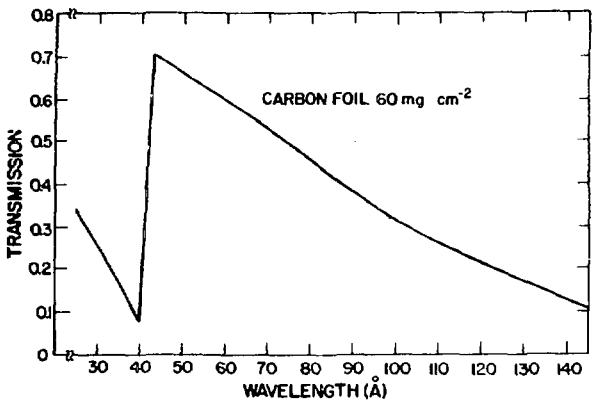

Fig. 4. Transmission vs wavelength for a thin carbon foil, 60 mg cm^{-3}, computed from absorption cross sections given by Henke (Ref. 18).

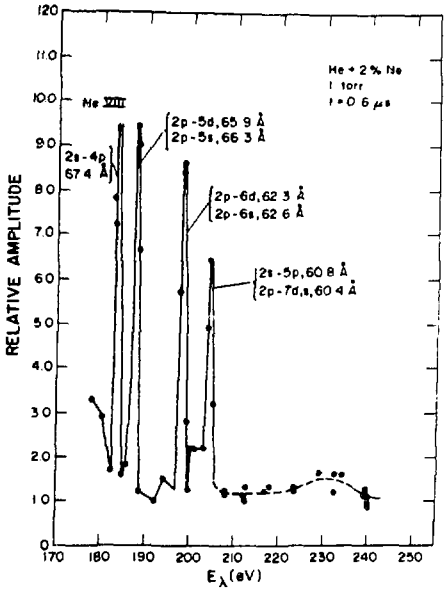

Fig. 6. Observed emission intensity vs photon energy. The θ-pinch was operated at the conditions of Fig. 5. Each point represents a separate shot of the bank, with the signal read at the peak value at t = 0.6 μs, with E$_\lambda$ set at the value plotted.

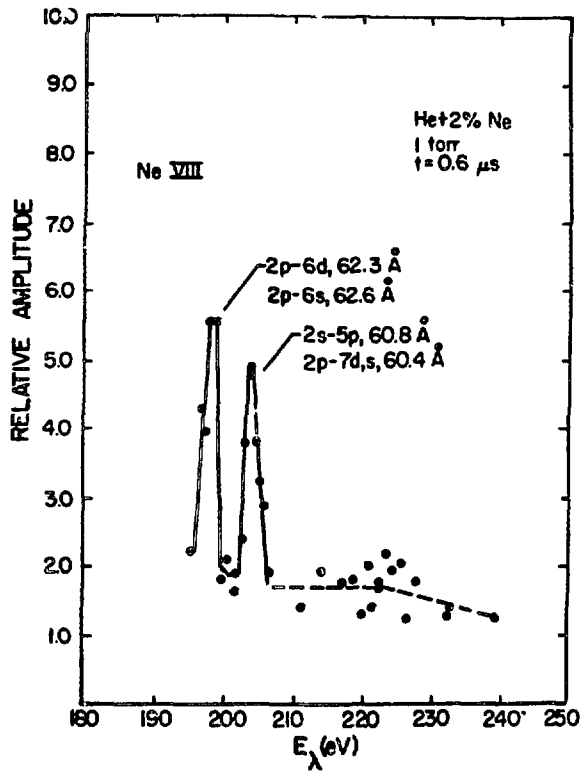

Fig. 7. Observed emission intensity vs energy. This is a partial preliminary scan, with an old θ-tube, taken at conditions similar to those in Figs. 5 and 6.

C. The Plasma Density and Temperature

The plasma was diagnosed using a pulsed ruby laser aimed down the Z-axis to give shadowgraphs of the diameter of the dense plasma. The technique was described in detail in Ref. 13. It has been our experience[4,13] that the high-density θ-pinch compresses with a sharp density gradient at the radial boundary so that ruby laser shadowgraphs give a good measure of the plasma radius. Figure 8 shows typical shadowgraphs obtained in the present work. Figure 9 shows a plot of θ-pinch radius vs time for the series of shadowgraphs that were taken to diagnose the case of helium + 2% neon at 1.0 torr used for the spectral scans in Figs. 6 and 7.

It is seen that the plasma compresses radially to a minimum diameter about 0.57 to 0.60 μs after start of the B field. Then it starts to expand and goes unstable at 0.7 to 0.8 μs.

If we assume that all the fill gas is swept up by the pinch, that all the helium is fully ionized, and that all the neon is Ne VIII, a maximum plasma density of $0.90 \pm 0.09 \times 10^{18}$ cm^{-3} is inferred from the minimum radius of Fig. 9 at 0.58 μs. The validity of the assumption of complete sweep up of helium was verified in Ref. 13.

A measure of the plasma temperature was obtained by the method[9] of observing the line/continuum ratio of the 4686-A He II line as had been done in earlier experiments.[4,6] The plasma was observed with a 0.5-m JACO monochromator and photomultiplier used in radial view in place of the VUV monochromator. The photomultiplier signal was recorded on a Tektronix 556 oscilloscope, and a separate shot of the θ-pinch was observed for each setting of the wavelength dial. Figure 10 shows the line profile obtained at t = 0.6 μs for the fill conditions, helium + 2% neon at 1.0 torr, used in the case of Figs. 6, 7, and 8.

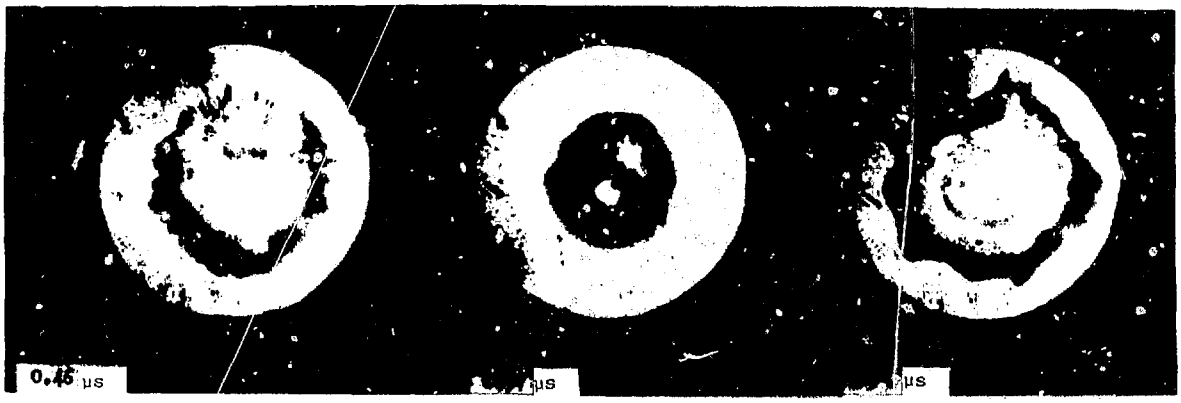

Fig. 8. Shadowgraphs taken with a ruby laser showing a radial view of the θ-pinch operated at the conditions of Figs. 5 and 6. Each shadowgraph was taken for a separate shot of the bank with the laser set at the time indicated.

The ratio of line to 100 A of continuum in Fig. 10 is 1.85 ± 0.2, which implies a temperature of 25 ± 4 eV, using the calculations of Merts and Magee[19] for helium + 2% neon.

The half-width at half maximum in Fig. 10 is $\delta_{1/21/2} = 5.0 \pm 0.5$ A. Using the formula of Sternheimer as discussed in Ref. 13, this gives an electron density of $(4.5 \pm .4) \times 10^{17}$ cm^{-3}.

The 4686-A line profile data of Fig. 10 were the last data taken in the present work; they were taken with a spare discharge tube (replacing the standard tube that had cracked), which had an inside diameter that was 5% smaller than the standard tube. We could expect the T_e and n_e values observed in Fig. 10 to be perhaps 5-10% smaller than for the case of the standard tube.

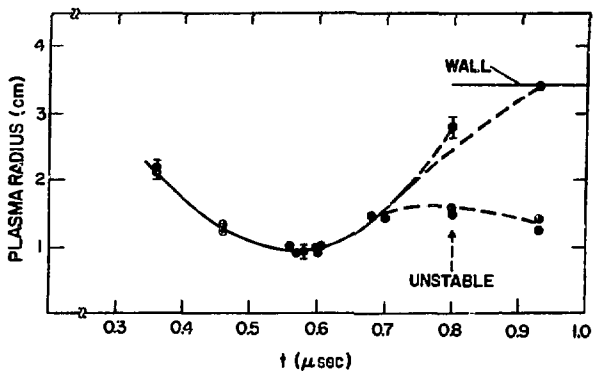

Fig. 9. Plasma radius vs time obtained from laser shadowgraphs like those in Fig. 8, with the θ-pinch operated at the conditions of Figs. 5 and 6. Each point is obtained from a shadowgraph for a separate shot of the bank.

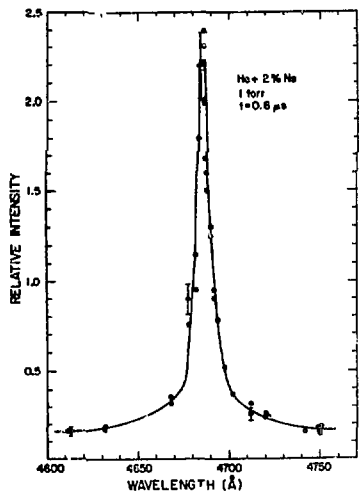

Fig. 10. Experimental profile of the He II 4686-A line emission from the θ-pinch operated at conditions of Figs. 5 and 6. The plasma is observed radially with the 0.5-m JACO monochromator and photomultiplier detector. Each point is the pulse height at t = 0.6 μs for a separate shot with the wavelength set at the value plotted.

We note that the electron density obtained from the He II line width was a factor of 2 smaller than that inferred from the measured plasma radius. This difference is greater than the errors assigned to each measurement. Each of the following factors may contribute to the difference: (a) the neon may not be swept up as completely as the lighter helium, (b) the tube diameters were slightly different, as mentioned above, and (c) the formula used to obtain n_e from $\epsilon_{1/21/2}$ has not been tested above 20 eV. No one of these factors is believed sufficient to fully explain the discrepancy. It would be desirable to repeat both measurements, at identical pinch conditions, in any case where the accuracy of the electron density measurement needs to be improved.

D. Comparison with an MHD θ-pinch Model

The observed properties of the θ-pinch may be compared with predictions[20] of the MHD pinch code Raven, developed by T. Oliphant, TD-2. The Raven code has been under development for some time for use[21] in

analysis of a high-density Z-pinch and other high-density plasma experiments. Using the θ-pinch drive conditions of this experiment and a pure helium gas fill of 1 torr, a typical Raven calculation predicts that the first bounce compression occurs about 0.64 μs after start of the B_z drive field. The electron density is 0.85 x 10^{18} cm^{-3} and the radius is 1.2 cm. These values compare favorably with the observed values of Fig. 9, where the first bounce occurs at 0.58 μs, at a radius of 0.95 cm, and at an electron density of 0.9 x 10^{+18} cm^{-3}.

The Raven calculation, which does not account for the effect of the 2% neon seed gas, predicts an electron temperature of ~60 eV (at r = 0) at peak compression (0.64 μs). This is substantially higher than the value of 25 eV obtained from the line/continuum ratio in Fig. 10. Since the 25-eV value measured with Fig. 10 agreed with the ~27 eV value observed in Fig. 14 from the relative intensities of the higher lying Ne VIII levels, we conclude that this is a reasonably accurate value. Thus the Raven prediction gives a factor of ≥2 higher value of T_e than the observed value. Much of the discrepancy may be because of the energy that goes into ionization and radiation due to the 2% neon seed gas. Otherwise, Raven gives a reasonably accurate description of this high density θ-pinch implosion.

IV. DISCUSSION OF RESULTS

A. Comparison of the Observed and Predicted Spectra

We now compare the results of the spectral observations of Figs. 6 and 7 with the theoretical predictions of the absorption calculations of Merts and Magee.[8] As presented in Fig. 1, these calculations give the relative amplitudes of the lines, fb edges, and continua, for the case of the resolution, or calculational band width, used in the code. For the case of Fig. 1, at T_e = 25 eV, this resolution was 0.25 eV. In Fig. 6, the resolution of the experimental data was 0.49 A (2.0 eV at E_λ = 220 eV). For comparison with the experiment, the relative magnitudes of the continua and fb edges in Fig. 1 are multiplied by the ratio of the resolution functions, (2.0 eV/0.25 eV) = 8, relative to the lines. All the magnitudes are corrected for the relative transmission of the carbon foil used, shown in Fig. 4. Figure 11 shows the results of these corrections to the relative theoretical emission intensities.

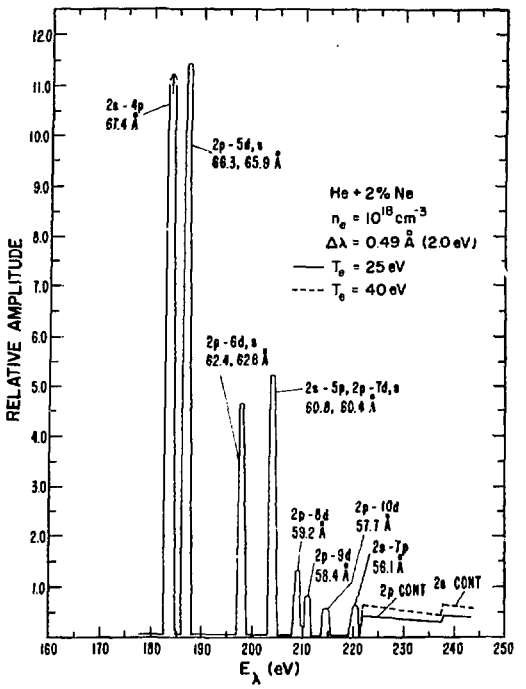

Fig. 11. Theoretical emission vs photon energy calculated using the resolution of the experiment. The theoretical curve of Fig. 1 has been corrected for the experimental resolution used in the data of Fig. 6 ($\Delta\lambda$ = 0.49 A, 2.0 eV). The solid curve is for 25 eV. The dotted curve is for 40 eV.

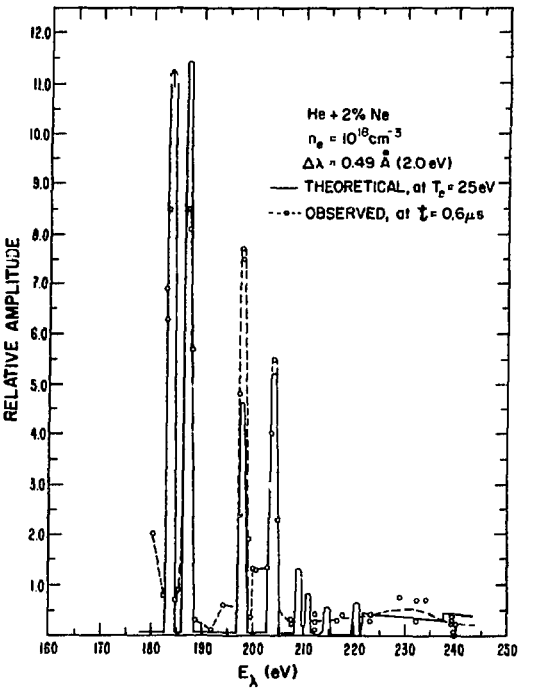

Fig. 12 Comparison of theoretical emission spectra of Fig. 11 with the experimental results of Fig. 6 with stray light subtracted. The theoretical amplitudes in Figs. 11 and 12 were normalized to the observed strengths of the NeVIII 2p-5d and 2p-6d lines.

In Fig. 11, all intensities have been multiplied by a constant factor so that the average magnitude of the 2p - 5d,s (66.3-, 65.9-A) line and the 2p - 6d,s (62.4-, 62.6-A) line is the same as the average magnitude of these two lines shown in the experimental data on Fig. 6. In Fig. 11 the solid curve shows the theoretical relative magnitudes of the lines and fb edges for the case of T_e = 25 eV. The dotted line shows the expected relative strength of the 2p and 2s edges calculated for T_e = 40 eV, all other conditions remaining the same.

Figure 12 shows the comparison of the observed spectral scan of Fig. 6 with the theoretical predictions given in Fig. 11. The stray light level seen in Fig. 6 has been estimated and subtracted from the amplitude of each experimental point plotted in Fig. 12.

Figure 12 most directly shows the comparison of the magnitude expected for the 2p edge relative to the observed magnitudes of the 2p - 5d,s and

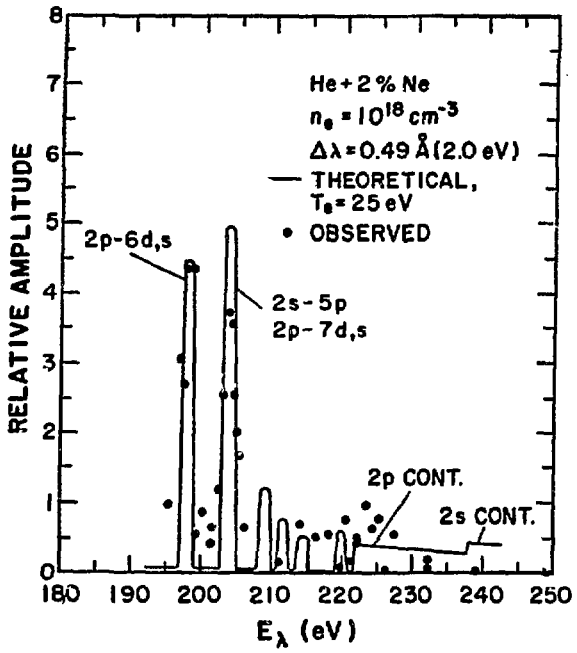

Fig. 13. Comparison of the theoretical and experimental spectra. The solid line is the theoretical curve, using relative intensities from Fig. 11. The plotted points are the experimental points of Fig. 7 (old tube) with a constant estimated value for the stray light subtracted. The theoretical relative amplitudes were normalized to the observed strength of the 2p-6d, s line. The theoretical line is for T_e = 25 eV.

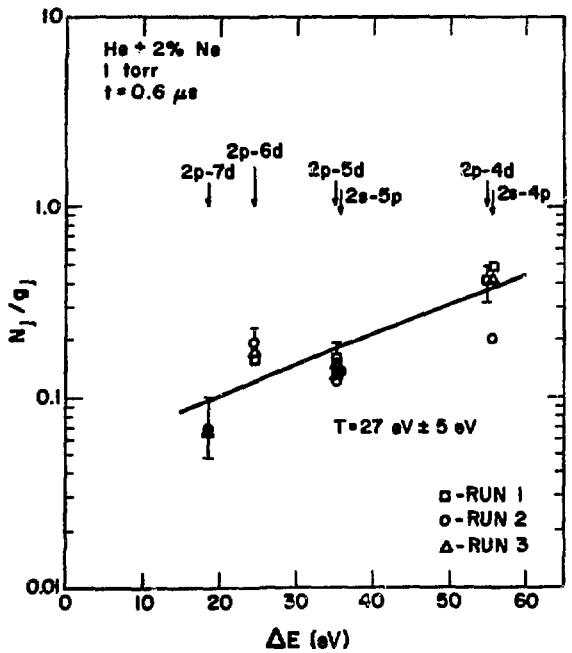

Fig. 14. Plot of $\ln N_j/g_j$ vs ΔE for the same plasma conditions as in Figs. 5 and 6. These quantities are defined in Eqs. (5) and (7). Each plotted point was obtained from the experimental amplitude assigned to each line from the scan for each run and corrected for the carbon filter transmissions. The individual runs are discussed in the text. The straight line drawn through the points represents an average slope for these data of 27 ± 5 eV.

2p - 6d,s lines. The theoretical and experimentally observed sums of the unresolved 2p - 7d,s and 2s - 5p lines are also compared in Fig. 12.

The time-resolved scan giving the data of Figs. 6 and 12 was not taken in enough detail to have observed the weak lines 2p - 8, 9, or 10, or the 2s - 7p line, but all of these lines were observed as very weak lines on film, for the plasma condition T_e = 40 eV and $n_e = 6 \times 10^{17}$, as reported in reference 4. In Fig. 12, the seven experimental points in the range, 206 < E < 220 eV mostly fall between the weak Ne VIII lines and thus their average value (0.25 units) is used to represent the background level there. The 12 experimental points in the range 221 < Eλ < 240 eV all fall where the jump owing to the predicted f b edges occur, so their average value (0.35 units) may represent the background plus continuum edge there. In Fig. 6, the shot-to-shot variations in the data indicate that an error of

about ±0.2 units should be assigned to the points between and above the strong lines. Errors of ± 25% may be estimated as applying to the relative strengths of the strong lines observed in Fig. 6.

With these errors, it appears in Fig. 12 that we should have just observed the 2p edge with the present data. Failure to do so may be just within the experimental errors. At any rate, the accuracy of the experiment is such that we can say that the strength of the 2p edge is not a factor of 2 larger than predicted.

When this work was first reported,[7] the theoretical prediction for the strength of the 2p edge relative to the strengths of the observed 2p - 5d,s and 2p - 6d,s lines was considerably larger than given in Figs. 1 and 11. We concluded then that the predicted edge must have been a factor of 2 or 3 too large compared to the experiment. Since that time, an error of X2 was found in our interpretation of the strengths of the lines relative to the continua in the opacity code printout. In addition, when comparing intensities of lines to continua, Merts and Magee found an error of π for the strengths of the narrow lines in their opacity code that was used for this calculation. The result is that in Figs. 1 and 11, the lines are a factor of 2π stronger relative to the continua, at a given temperature, than we reported earlier.[7]

For completeness, we show in Fig. 13, the expected amplitudes of the 2p and 2s edges for the data of Fig. 7, taken with an older discharge tube and more stray light background. The comparisons in Fig. 13 are made in a way similar to those in Fig. 12. The accuracy of the data points in Fig. 13 is not sufficient to observe the 2p edge at the strength predicted, but again we can say it is not a factor of 2 or 3 larger than predicted.

B. The LTE Condition

We now want to determine to what extent the experiment may have satisfied the conditions required for LTE as discussed in II-C.

We make use of an expression[9,22] for the intensity of a spectral line

$$I(\omega) \propto \hbar\omega_{ji} \frac{N_j}{g_j} \sum_{\ell} g_\ell A_{ji} \quad , \tag{4}$$

where N_j = number density of ions in the upper state of the line and A_{ji} = transition probability for spontaneous emission from state j to state i.

Equation (4) may be written

$$\frac{N_j}{g_j} \propto \frac{I(\omega)}{h\omega_{ji} \sum_{\ell} g_{\ell} A_{ji}} , \tag{5}$$

where the summation $\Sigma\, g_{\ell} A_{ji}$ is over all ℓ values of the upper state j.

If the upper states j of say Ne VIII are in equilibrium with the ground state of the next higher ion state Ne IX, we may write[22]

$$\frac{N_j}{g_j} = \frac{N_{\text{Ne IX}}}{g_{\text{Ne IX}}} \exp\left(\frac{\Delta E}{kT}\right), \tag{6}$$

where Ne IX is in the ground state and where

$$\Delta E = E_{ion} - E_j . \tag{7}$$

In Eq. (7), E_{ion} is the ionization energy above the ground state of Ne VIII, and E_j is the energy of the level j above the ground state of Ne VIII, so that ΔE is the energy interval from the upper state j to the ground state of Ne IX.

Then if, for two or more observed lines, we plot

$$\ell n \frac{N_j}{g_j} \quad \text{vs} \quad \Delta E , \tag{8}$$

the slope will give $\frac{1}{kT}$, where T is the excitation temperature for the lines plotted. If the value of T obtained from such a plot is equal to the electron temperature, then we are in LTE for the levels j for which this is the case.

In Fig. 14 we have plotted $\ln N_j/g_j$ vs ΔE for the same plasma condition as used in the data of Fig. 6. The values N_j/g_j are obtained from relative intensities $I(\omega)$ of the observed lines from the higher lying levels. Run 2 comes from the data of Fig. 6, and runs 1 and 3 come from additional runs for which the lines were studied with more shots, and the edge was not searched for. In the case of run 3, a wider slit width was used to increase the intensity of the lines and reduce the shot-to-shot variations.

In Fig. 14, the points plotted for the 2s - 5p and 2p - 7d,s lines are obtained from the observed intensity of the unresolved 60.8 and 60.4 A lines. This intensity is divided between these two lines by the ratio obtained from the values of $(\Sigma g_\ell A_{ji})/2n^2$ for the two lines. The values used for $g_\ell, A_{j,i}$, n, and $\Sigma g_\ell A_{ji}$ for each line are given in the Appendix. The slope in Fig. 14 gives an excitation temperature of 27 ± 5 eV, in good agreement with the temperature of 25 eV obtained from the He II 4686-A line/continuum ratio in Fig. 10. We take this agreement as good evidence that we are in LTE, or approaching LTE, for the lines for which $n \geq 4$.

For comparison we consider a case for which the electron density was an order of magnitude lower and the electron temperature was substantially higher. In data reported earlier,[17] the time-resolved spectra was observed for the case of Scyllar operated at 1/3 bank energy (B_{max} = 45 kG) with a gas fill of helium + 2% neon at 150 mT. In Fig. 15 we show the spectra observed for this case at t = 0.9 μs. The lines 2s - 3p to 2s - 5p, and 2p - 4s to 2p - 7d were observed. The temperature and density of this plasma was diagnosed[17,14] by Thomson scattering and holographic interferometry using a ruby laser. At 0.9 μs, T_e was 130 eV and n_e was 10^{17} cm^{-3}. Using the method discussed for Fig. 14, a plot of $\ln N_j/g_j$ vs ΔE was made for the lower density case and is shown in Fig. 16.

In Fig. 16, we have drawn a straight line with a slope corresponding to T_e = 130 eV through the data points, normalized to the average intensity of the high-lying levels 2p - 7d and 2p - 6d. The plotted points for the lower levels clearly do not fall on the T_e = 130 eV slope. We conclude that we are substantially out of LTE for the levels with upper states n = 5 and n = 4.

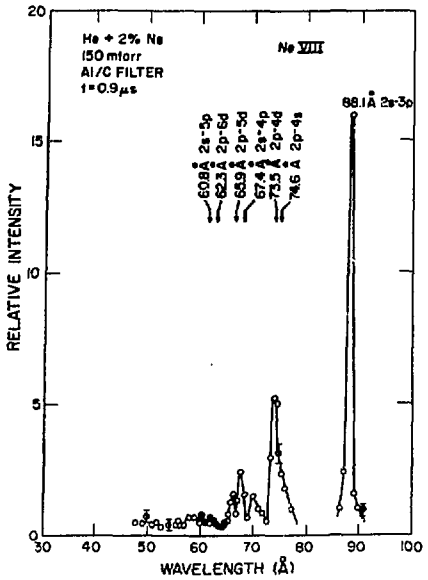

Fig. 15. Observed intensity vs wavelength (λ) for the case of Scyllar operated at 1/3 bank (B = 45 kG) with a fill of helium + 2% neon at 150 mT and reported in Ref. 17. Laser diagnostics gave T_e = 130 eV and $n_e = 10^{17}$ cm^{-3}.

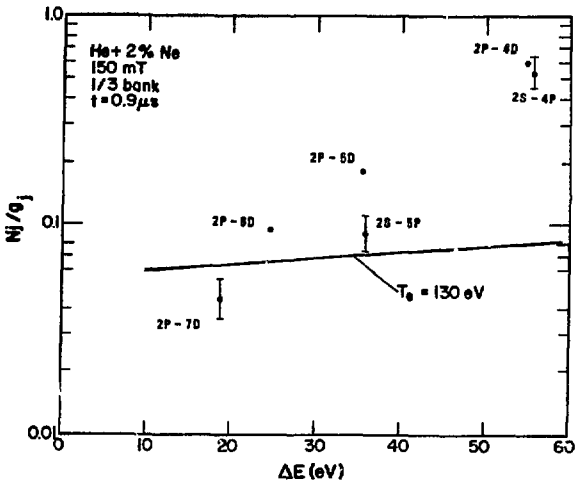

Fig. 16. Plot of ℓn N_j/g_j vs ΔE for the plasma conditions and using the data of Fig. 15. Individual line amplitudes have been corrected for the thin film filter (C/Aℓ) transmissions. The straight line slope shown represents the electron temperature, T_e = 130 eV, measured by laser scattering.

From comparison of the data of Figs. 16 and 14, it appears that by increasing the electron density from 10^{17} cm^{-3} to 10^{18} cm^{-3} and by decreasing the electron temperature from ∿130 to ∿25 eV, we have progressed from a non-LTE case to a case closely approaching LTE for $n \geq 4$.

C. Conclusions and Recommendations

The results of the present experiment lead to three conclusions.

(1) The approach to LTE, indicated by comparison of the ℓn(N_j/g_j) vs ΔE plots as the electron density was increased a factor of 10, indicates that the equilibrium conditions of the experiment were reasonably well satisfied. This conclusion is supported by the agreement between the excitation temperatures (∿25 eV) obtained from the He II 4686-A line/continuum ratio and from the slope of the ℓn N_j/g_j vs ΔE plot.

(2) The accuracy of the shot-to-shot scan of the spectral region of the 2p fb recombination edge of Ne VIII was not sufficient to observe the edge. It was sufficient, however, to show that the edge was not a factor of 2 or more greater than was predicted by the opacity code. The scan also was sufficiently accurate to lead to a reanalysis of the emission calculations and thus to the discovery of an error of a factor of π in the

strength of the narrow lines calculated in the particular opacity code used for this comparison. Rosseland mean opacities, however, are not affected significantly by this error.

(3) The present experiment and comparison with theory demonstrate a method for testing opacity calculations.

These results suggest the following recommendations:

(1) The present experiment came very close to observing the Ne VIII fb edge, for a case, that is θ-pinch, for which the plasma is relatively homogeneous and the electron temperature is Maxwellian and meaningful. Free-bound edges have been observed on film spectra[23,24] for very high density, inertially confined plasmas produced with lasers. In such cases, it has sometimes been more difficult to assign an electron temperature to the observed spectra. It is recommended therefore to use the methods of the present experiment with higher density magnetically confined plasmas, perhaps created in a laser-heated θ-pinch, or solenoid, experiment[25] for which electron densities of 10^{19} cm^{-3} might be obtained and diagnosed at relevant temperatures.

(2) Higher density plasmas (10^{20}-10^{22} cm^{-3}) currently are being created by laser implosion of pellets,[24,26] Z-pinches,[27] etc. Such plasmas could be appropriate samples for opacity studies if their electron temperature and homogeneity can be sufficiently well determined.

(3) The method of determining the plasma temperature from the slope of the $\ln N_j/g_j$ vs ΔE curves for the higher lying levels of Ne VIII suggests that we might use neon as a seed to determine the temperature in a plasma seeded with a more complicated high-Z element, such as iron, for which it is desired to study the opacity. The slope of the high-lying levels of neon could be calibrated in a helium plasma (such as in the present experiment), then the neon used to seed the iron plasma at a comparable electron temperature and density to maintain the LTE condition. It would, of course, be necessary to choose conditions for which there were no strong iron lines interfering with the neon lines being used for the measurement.

V. SUMMARY

Radiation from a neon-seeded high-density θ-pinch has been observed and compared with theoretical predictions based on opacity calculations. The θ-pinch was created in a 25-cm-long coil by a 90-kG axial drive field with a quarter period of 3.0 μs. The gas fill was helium + 2% neon at 1 torr.

The time-resolved emission spectra were observed in the VUV range, in radial view, with a 2.2-m grazing incidence vacuum monochromator equipped with p-terphenyl scintillator and photomultiplier. The predominant emission observed came from the stronger lines of Ne VIII.

The weak high-lying levels of the Ne VIII, up to n = 7, were observed with the aid of thin carbon foils, which filtered out stray light. The plasma temperature was measured to be 25 eV by observing the He II 4686-A line/continuum ratio. The electron density was determined to be 0.9×10^{18} cm^{-3} from the plasma radius observed with laser shadowgraphs. Analysis of the intensities of the high-lying Ne VIII levels gave a temperature of ≈27 eV and indicated that the LTE requirements of the experiment were satisfied. This analysis demonstrated the use of these higher lying levels as a temperature diagnostic.

A search was made for the 2p free-bound recombination edge in Ne VIII, using the VUV monochromator. The predicted strength of this edge, relative to the observed strength of the 2p - 5d and 2p - 6d lines, was calculated theoretically using values of the absorption cross section from an opacity code. The edge was not observed, but comparison of the calculations with the experimental data indicated that the strength of the fb cross section must be approximately equal to or less than that given by the opacity code.

ACKNOWLEDGMENTS

The suggestions and theoretical computations of A. L. Merts, N. H. Magee, and W. F. Huebner were essential to the choice of parameters and interpretation of results for this work and are gratefully acknowledged.

E. Källne and L. A. Jones played an invaluable role in the development of the time-resolved VUV spectroscopy used here and contributed many helpful ideas during the course of the work. The suggestions of H. R.

Griem were invaluable to the interpretation of the results, particularly with regard to the LTE analysis. The application of the Raven MHD code to this experiment by T. A. Oliphant is appreciated.

The efforts of Ralph Roy in refurbishing and operating the 180 kJ capacitor bank, keeping it in repair, and helping with the diagnostics were invaluable to the completion of the experiments and are greatly appreciated.

REFERENCES

1. W. F. Huebner, J. Quant. Spectr. Rad. Tr. 7, 949 (1967).

2. N. H. Magee, A. L. Merts, and W. F. Huebner, Astn. J. 196, 617 (1975).

3. H. Mayer, "Methods of Opacity Calculations," Los Alamos Scientific Laboratory report LA-647 (1948).

4. D. B. Thomson, A. G. Bailey, and R. Engleman, Jr., "Vacuum Ultraviolet Emission from a Neon-Seeded Theta Pinch," Los Alamos Scientific Laboratory report LA-5466-MS (March 1974).

5. A. L. Merts, private communication, 1972.

6. D. B. Thomson, L. A. Jones, A. G. Bailey, and R. Engleman, Jr., "Characteristics of High Density θ-Pinches Seeded With Selected High-Z Elements," Pulsed High Beta Plasmas, D. E. Evans, Ed., (Pergamon Press, Oxford & New York, 1976), pp. 207-213.

7. D. B. Thomson, "VUV Emission Near the Ne VIII 2p Recombination Edge from a High Density θ-Pinch," Bull. Am. Phys. Soc., Ser II, 22, No. 9 (1977) Paper 8A14.

8. A. L. Merts and N. H. Magee, private communication, 1977, 1978.

9. H. R. Griem, Plasma Spectroscopy, (McGraw-Hill Book Co., New York, 1964), pp. 114-171.

10. A. L. Merts and W. Matuska, Jr., Los Alamos Scientific Laboratory report LA-5380 (1973).

11. D. B. Thomson, A. G. Bailey, R. Engleman, Jr., "VUV Emission from a Neon Seeded θ-Pinch," Bull. Am. Phys. Soc. Ser II, 17 No. 11 (1972) Paper 8F11

12. R. Engleman, Jr., D. B. Thomson, and D. A. Monaghan, "Vacuum Ultraviolet Emission from Argon, Krypton, and Xenon in a Radial-Viewed Theta Pinch," Los Alamos Scientific Laboratory report LA-6275-MS (1976).

13. L. A. Jones, E. Källne, D. B. Thomson, "High Density Measurements of the Stark Broadened Profile of the HeII 4686A Line," J. Quant. Spectr. Rad. Tr. 17, 175 (1977).

14. L. A. Jones, E. Källne, and D. B. Thomson, "Measurement of the Total Collisional Ionization Rates of Ne VI, VII, and VIII," J. Phys. B 10, 187 (1977).

15. E. Källne and L. A. Jones, "Measurements of the Ionization Rates of Li-Like Ions," J. Phys. B 10, 3673 (1977).

16. R. U. Datla, L. A. Jones, D. B. Thomson, "Temperature Diagnostics Using Li-Like Satellites," 2nd Topical Conference on High-Temperature Plasma Diagnostics, APS Santa Fe, NM, March 1-3, 1978, Los Alamos Scientific Laboratory report LA-7160-C. Paper D-13.

17. D. B. Thomson and E. Källne "Time Resolved VUV Spectra from High-Lying Levels of Ne VIII in a Theta Pinch," Bull. Am. Phys. Soc. Ser. II 21, No. 9, October 1976, Paper 5S4.

18. B. L. Henke and R. L. Elgin, Advances in X-Ray Analysis, Vol. 13, (Plenum Press, NY, 1970).

19. A. L. Merts and N. H. Magee, Jr., "Determination of Temperature and Density in Low Temperature Dense Plasmas Using Line to Continuum Intensity Ratios," Bull. Am. Phys. Soc., Ser. II, 17, No. 11 (1972) Paper 8 F12.

20. T. A. Oliphant, private communication, 1977.

21. J. H. Brownell and T. A. Oliphant, "Numerical Study of a High Density Z-Pinch," Bull. Am. Phys. Soc. 23, No. 7 (1978) Paper 6T3.

22. Larry A. Jones, "Measurement of Excited States Number Densities of Oxygen and Nitrogen in a Non-Equilibrium Plasma," J. Quant. Spectr. Rad. Tr. 15, 1083 (1975).

23. D. J. Nagel, "X-Ray Emission From High Temperature Laboratory Plasmas," Advances in X-Ray Analysis, 18 1 Plenum Press, New York (1975).

24. K. B. Mitchell, et al., private communication (1979).

25. Alan L. Hoffman and Edward A. Crawford, "Laser Heating of Magnetically Confined Plasmas for X-Ray Production, Phase III," DNA-3963F, Mathematical Sciences Northwest, Inc., Bellevue, WA 98009 (April 1976).

26. K. B. Mitchell, D. B. van Hulsteyn, G. H. McCall, Ping Lee, and H. R. Griem, "Compression Measurements of Neon Seeded Glass Microballoons Irradiated by CO_2 Laser Light." Phys. Rev. Lett. 42, 232 (1979).

27. L. A. Jones, J. E. Hammel, W. C. Nunnally, and D. B. Thomson, private communication, 1978.

APPENDIX A

VALUES USED FOR ANALYSIS OF THE Ne VIII LINE RATIOS

Intensity of a Spectral Line is

$$I(\omega) \alpha \hbar \omega_{ji} \frac{N_j}{g_j} \sum_{\ell} g_\ell A_{ji} \quad , \tag{A-1}$$

where

ω_{ji} = emission frequency,
i,j = lower and upper states,
$A_{j,i}$ = atomic transition probability from state j to state i,
N_j = number density of the upper state,
g_j = total degeneracy for the quantum number n_j of the state j, and
g_ℓ = degeneracy for a given ℓ value of the upper state.

These quantities are given by the following expressions.

$$g_j = 2n_j^2 \tag{A-2}$$

$$g_\ell = 2\ell + 1 \tag{A-3}$$

$$A_{ji} = f_{ij} \frac{6.67 \times 10^{15}}{\lambda^2} \left(\frac{g_i}{g_j}\right) \quad . \tag{A-4}$$

Equation (A-4) is taken from Wiese, Smith, and Glennon "Atomic Transition Probabilities," Table III, National Bureau of Standards report NSRDS-NBS-4, p. X. The f_{ij} are obtained from Ref. 3.

See Table A-I for values.

TABLE A-I

VALUES

Transition	λ (A)	n_j	g_ℓ	g_j	A_{ji} (S^{-1})	$\sum_\ell g_\ell A_{ji}$	$\hbar\omega_{ji}$[a] (eV)	ΔE[b] (eV)
2p - 4d	73.50	4	5	32	0.090	0.450	168.3	54.9
2s - 4p	67.39	4	3	32	0.0502	0.151	183.5	55.6
2p - 5d	65.86	5	5	50	0.0411	0.2116	187.8	35.3
2p - 5s	66.30	5	1	50	0.00614		186.6	
2s - 5p	60.8	5	3	50	0.0250	0.075	203.4	35.7
2p - 6d	62.33	6	5	72	0.0224	0.115	198.3	24.7
2p - 6s	62.58	6	1	72	0.00314		197.6	
2p - 7d	60.38	7	5	98	0.0135	0.070	204.9	18.7
2p - 7s	60.49	7	1	98	0.00197		204.7	

a. $\hbar\omega_{ji} = \frac{12367}{\lambda}$.

b. $\Delta E = E_{ion.} - E_j$

where $E_{ion.} = 239.09$ eV for Ne VIII

and where $E_j = \hbar\omega_{ji}$ for i = 2s

$E_j = \hbar\omega_{ji} + E_i$ [$E_i = 16.0$ eV for i = 2p, Ne VIII] .